Kinetics and Regulation of Mammalian NADH-Ubiquinone Oxidoreductase (Complex I)

Xuewen Chen,[△] Feng Qi,[△] Ranjan K. Dash, and Daniel A. Beard*
Biotechnology and Bioengineering Center and Department of Physiology, Medical College of Wisconsin, Milwaukee, Wisconsin

ABSTRACT NADH-ubiquinone oxidoreductase (Complex I, European Commission No. 1.6.5.3) is one of the respiratory complexes that generate the proton-motive force required for the synthesis of ATP in mitochondria. The catalytic mechanism of Complex I has not been well understood, due to the complicated structure of this enzyme. Here, we develop a kinetic model for Complex I that accounts for electron transfer from NADH to ubiquinone through protein-bound prosthetic groups, which is coupled to the translocation of protons across the inner mitochondrial membrane. The model is derived based on the tri-bi enzyme mechanism combined with a simple model of the conformational changes associated with proton transport. To study the catalytic mechanism, parameter values are estimated by analyzing kinetic data. The model is further validated by independent data sets from additional experiments, effectively explaining the effect of pH on enzyme activity. Results imply that matrix pH significantly affects the enzyme turnover processes. The overall kinetic analysis demonstrates a hybrid ping-pong rapid-equilibrium random bi-bi mechanism, consolidating the characteristics from previously reported kinetic mechanisms and data.

INTRODUCTION

NADH-ubiquinone oxidoreductase (Complex I, European Commission No. 1.6.5.3) catalyzes the reduction of lipid-soluble coenzyme Q (ubiquinone, CoQ) by water-soluble $NADH^{2-}$, which is the first step in the mitochondrial respiratory system,

$$NADH^{2-} + CoQ + H_x^+ + 4H_x^+ \rightleftharpoons QH_2 + NAD^- + 4H_i^+, \quad (1)$$

where subscripts x and i indicate protons inside and outside of the matrix, respectively. Therefore, this biochemical reaction represents two coupled processes: reduction of ubiquinone (CoQ) to ubiquinol (QH_2) by $NADH^{2-}$, transferring one free hydrogen ion to ubiquinone, and transport of four hydrogen ions out of the matrix across the mitochondrial inner membrane. Complex I, illustrated schematically in Fig. 1 *A*, is an L-shaped protein complex located in the mitochondrial inner membrane, with one arm protruding into the matrix space (1,2). It contains at least 41 subunits and 9 redox cofactors (a flavin mononucleotide and eight iron-sulfur (Fe-S) clusters) in mammalian cardiac mitochondria, more than any other complex in the electron transport system (3,4). These subunits are grouped into three modules, the NADH dehydrogenase module, the hydrogenase module, and the proton transporter module (1). The latter two modules couple by a yet unknown mechanism and are linked with a redox-driven proton translocation. The mechanism by which electron transfer and proton pumping are coupled via Complex I has not been established, but it has been suggested that it involves conformational changes (5,6).

Recently, a number of in vitro experiments have been performed in an attempt to understand the catalytic mechanism of Complex I. Fato et al. (7) investigated the kinetics of Complex I from bovine heart mitochondrial membrane using CoQ_1 and 6-pentylubiquinone as artificial electron acceptors and proposed a ping-pong catalytic mechanism for the enzyme. Nakashima et al. (8) used CoQ_1 as the electron acceptor to analyze the activity of Complex I purified from bovine heart muscle. They proposed an ordered sequential mechanism with CoQ_1 binding in the first step and Q_1H_2 releasing in the last step. Hano et al. (9) also assumed that the kinetics of Complex I obeys an ordered sequential mechanism when they used DQ as the electron acceptor, and suggested that the maximal enzyme activity at the saturating concentrations of DQ and $NADH^{2-}$ is not sensitive to pH. Sadek et al. (10) reported that pH and Ca^{2+} regulate the activity of Complex I from solubilized rat heart mitochondria.

The in vivo behavior of Complex I necessarily differs from that of purified Complex I in solution. One fundamental difference is that in vivo Complex I function is dependent on the electrostatic potential across the mitochondrial inner membrane (11–13). Thus, the membrane potential will have a direct effect on reduction of Q to QH_2 and transfer of protons from the matrix space to the intermembrane space. In addition, pH in the matrix space also affects the electron transport rate (9,11,14). The primary motivation of this work is to understand kinetic data reported by different groups in terms of a mathematical model using a unified catalytic mechanism that can characterize and predict Complex I behavior under different conditions, both in vitro and in vivo.

Submitted April 7, 2010, and accepted for publication June 22, 2010.

[△]Xuewen Chen and Feng Qi contributed equally to this work.

*Correspondence: beardda@gmail.com

Xuewen Chen's present address is Plant Biology Department, Michigan State University, East Lansing, MI.

Editor: Patrick Loria.

0006-3495/10/09/1426/11 $2.00

doi: 10.1016/j.bpj.2010.06.063

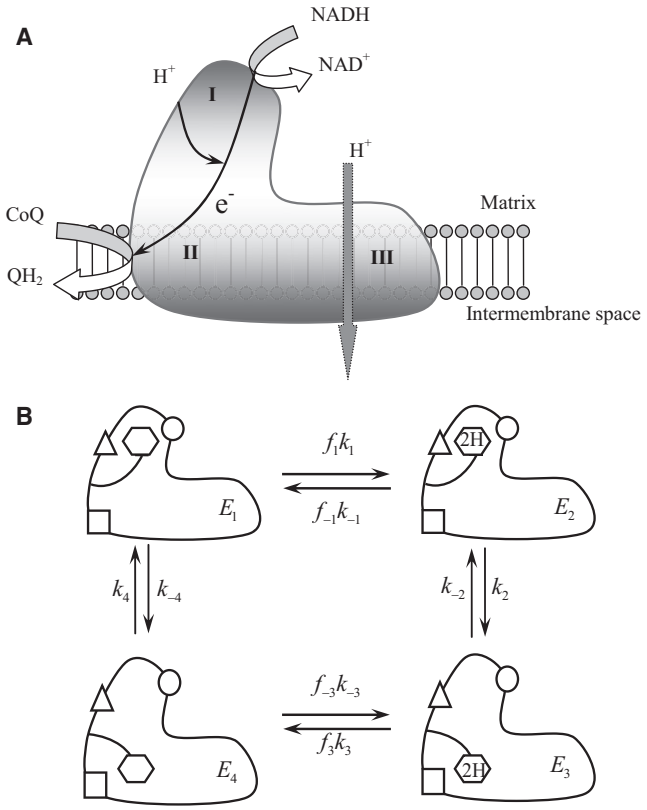

FIGURE 1 (*A*) Schematic representation of the mechanism of Complex I. The $NADH^{2-}$ dehydrogenase module (*I*) accepts electrons from $NADH^{2-}$ and transfers them to the hydrogenase module (*II*) via the flavin (FMN) and the iron-sulfur clusters (N1–N5). Further transfer to N2 and finally to ubiquinone (Q) is linked with a redox-driven proton translocation (*black arrows*). The conformational changes of the proton transporter module (*III*), which transfer protons from the matrix to the cytosol, are mediated by the overall electron transfer by a yet unknown coupling mechanism. (*B*) Kinetic scheme of the tri-bi enzyme mechanism in combination with the mechanism of conformational changes. The forward reaction is read in the clockwise direction. The enzyme has three binding sides: site 1 binds to the proton (*triangles*), site 2 binds to substrate A or the corresponding product P (*circles*), and site 3 binds to substrate B or the corresponding product Q (*squares*). It is assumed that the mechanism involves conformational changes that are accompanied by phenomenological transfer of the H_2 moiety from sites 1 and 2 to site 3.

Long-chain lipid-soluble electron acceptors (such as CoQ_{10}) are largely lipid-bound in vivo, as compared to those in aqueous solution. Due to the insolubility of natural ubiquinone in aqueous solutions, experimental assays are usually performed using the short-chain coenzyme Q homologs and analogs as substitutes. Fato et al. (7) evaluated the effects of using different soluble CoQ analogs, and concluded that the behavior of CoQ_1 is the most similar to that of CoQ_{10}, because electron transfer from $NADH^{2-}$ reduces CoQ_1 at the same rate it reduces CoQ_{10} occurring at or near the physiological CoQ_{10} site, so that CoQ_1 has kinetic rates comparable to those calculated from reduction of endogenous CoQ_{10}. In a similar way, based on a systematic examination of the assay conditions of Complex I in the mitochondrial inner membrane using a series of coenzyme Q homologs, such as CoQ_0, CoQ_1, and CoQ_2, and the analogs duroquinone and decylubiquinone, Estornell et al. (15) concluded that the CoQ_1 is the most suitable homolog.

One major motivation for developing a mechanistic model for Complex I function is that a model may prove useful to better understand the role of Complex I in superoxide ($O_2^{-\cdot}$) formation (16). The production of $O_2^{-\cdot}$ is reported to be much higher in Complex I when the net flux in Eq. 1 is in the reverse direction than when it is in the forward direction (17). The mechanism of this phenomenon is unknown. Lambert and Brand (11) found that $O_2^{-\cdot}$ production in isolated mitochondria from rat skeletal muscle is suppressed by rotenone and uncoupling agents, but not by nigericin. They suggested that the pH gradient across the mitochondrial inner membrane may play a role in $O_2^{-\cdot}$ production. Kussmaul and Hirst (14) measured $O_2^{-\cdot}$ production from pure Complex I isolated from bovine heart mitochondria. Their results show a positive correlation between the $NADH^{2-}/NAD^-$ ratio and $O_2^{-\cdot}$ production.

Another issue that may affect the analysis of in vivo Complex I activity is the $NADH^{2-}$ binding state. It has been reported that mitochondrial $NADH^{2-}$ is predominantly protein-bound, where NAD^- is mostly in the free state (18,19). Tischler et al. (19) estimated that the ratio of mitochondrial $NADH^{2-}_{free}$ to $NADH^{2-}_{total}$ in hepatocytes is in the range 8.5–22.5%, based on the lactate dehydrogenase redox couple at pH 7.0 and β-hydroxybutyrate dehydrogenase redox couple at pH 7.4. Therefore, it is important to account for $NADH^{2-}$ binding in the elucidation of Complex I catalytic mechanisms in vivo. Because of binding, the reported apparent K_m values of $NADH^{2-}$ are greater for submitochondrial particles (SMPs) and beef heart mitochondria (BHM) than for the purified enzyme: the latter is around 2 μM (8,9), only ~20% of the apparent K_m for SMPs (9.2 μM) and BHM (8.7 μM) (7).

In this work, we develop a mechanistic model to describe Complex I activity in purified enzyme experiments as well as in the intact mitochondria in vivo. The model is derived from a tri-bi enzyme mechanism combined with a model of conformational changes associated with proton transport across the inner mitochondrial membrane. Parameter values of the proposed kinetic model are estimated by analyzing available kinetic data; the model is validated based on independent data sets from additional experiments.

METHODS

In this section, we first introduce a general kinetic model for conformational change in a tri-bi enzyme mechanism. The model is then further developed to account for proton transport and $\Delta\Psi$ dependency to characterize the kinetic model of Complex I. Finally, we describe the method used to estimate the kinetic parameter values in the model.

Kinetic model for conformational change in a tri-bi enzyme mechanism

Complex I is a multisubunit and multiredox component enzyme. Structure studies imply that Complex I has an L-shaped structure consisting of a membrane domain and a peripheral arm (20), with the majority of the peripheral arm located in the matrix (21). Recent structure and evolution studies have elucidated a modular structure of Complex I. It contains an $NADH^{2-}$ dehydrogenase module, a hydrogenase module, and a transporter module (Fig. 1 *A*). The hydrogenase and transporter modules are known to be involved in proton translocation and act as redox-driven and conformation-driven proton pumps, respectively (22).

The kinetic equation of our model for Complex I catalytic reaction is derived from a tri-bi enzyme mechanism combined with a model of conformational change. The derivation is inspired by a previously developed model for transcarboxylase (23,24). The basic chemical reaction of the tri-bi enzyme mechanism has the form

$$\mathrm{A} + \mathrm{B} + \mathrm{H}^+ \rightleftarrows \mathrm{P} + \mathrm{Q}, \tag{2}$$

in which we have temporarily excluded the proton pumping component from the analysis. The model assumes that the enzyme has three binding sites: site 1 binds to the proton, site 2 binds to substrate A or the corresponding product P, and site 3 binds to substrate B or the corresponding product Q. In addition, it is assumed that the basic mechanism involves four conformational changes that accompany the transfer of a 2H moiety from sites 1 and 2 to site 3, as illustrated in Fig. 1 *B*.

Each binding state can exist in any one of the four conformational states illustrated in Fig. 1 *B*. The first site is either empty or proton-bound; the second site is either empty or bound to A or P; and the third site is either empty or bound to B or Q. Therefore, there are a total of 18 binding states associated with each of these four conformational states, yielding a total of $4 \times 18 = 72$ distinct states in the model. The 72 states are denoted as E^i_{xyz}, where $i \in \{1,2,3,4\}$ indicates the conformational state, $x \in \{\varnothing, \mathrm{H}\}$ indicates the site-1 binding state, $y \in \{\varnothing, \mathrm{A}, \mathrm{P}\}$ indicates the site-2 binding state, and $z \in \{\varnothing, \mathrm{B}, \mathrm{Q}\}$ indicates the site-3 binding state. Using the lower-case e^i_{xyz} to indicate a fraction in each state, we have

$$e^i_{\mathrm{total}} = \sum_{x \in \{\varnothing,\mathrm{H}\}, y \in \{\varnothing,\mathrm{A},\mathrm{P}\}, z \in \{\varnothing,\mathrm{B},\mathrm{Q}\}} e^i_{xyz}. \tag{3}$$

For each conformation, we assume the rapid equilibration between 18 bound states, which means that the binding processes are much faster than conformational changing processes:

$$e^i_{\mathrm{total}} = \left(1 + \frac{[\mathrm{H}^+]}{K_\mathrm{H}}\right)\left(1 + \frac{[\mathrm{A}]}{K_\mathrm{A}} + \frac{[\mathrm{P}]}{K_\mathrm{P}}\right)\left(1 + \frac{[\mathrm{B}]}{K_\mathrm{B}} + \frac{[\mathrm{Q}]}{K_\mathrm{Q}}\right) e^i_{\mathrm{free}}, \tag{4}$$

where $e^i_{\mathrm{free}} \equiv e^i_{\varnothing\varnothing\varnothing}$ indicates fraction of the free enzyme; K_H, K_A, K_P, K_B, and K_Q are the dissociation constants for H^+, A, P, B, and Q binding, respectively. It is assumed that these constants do not depend on the conformational state of the enzyme. (It has been shown that the binding events are not influenced by the electron transfer reaction inside the enzyme (9).) Furthermore, the presence of a reactant at one site does not influence the binding reaction at another, meaning that these constants are independent of each other. These simplifying assumptions are necessary to make the model tractable, and are validated by comparison of model prediction to experimental data.

We define f_1 and f_3 as the fractions in conformations 1 and 3 that may undergo forward conformational transformations to states 2 and 4. In a similar way, f_{-1} and f_{-3} are the fractions in conformations 2 and 4 that are able to undergo conformational transformation in the reverse direction (see Fig. 1 *B*). Specifically, the model mechanism requires that proton binding at site 1 and A binding at site 2 are necessary for transition from conformational state 1 to state 2. Therefore,

$$\begin{aligned} f_1 &= \frac{e^1_{\mathrm{HA}\varnothing} + e^1_{\mathrm{HAB}} + e^1_{\mathrm{HAQ}}}{e^1_{\mathrm{total}}} \\ &= \frac{\dfrac{[\mathrm{H}^+]}{K_\mathrm{H}}\dfrac{[\mathrm{A}]}{K_\mathrm{A}}}{\left(1 + \dfrac{[\mathrm{H}^+]}{K_\mathrm{H}}\right)\left(1 + \dfrac{[\mathrm{A}]}{K_\mathrm{A}} + \dfrac{[\mathrm{P}]}{K_\mathrm{P}}\right)}. \end{aligned} \tag{5}$$

In a similar way, we will have

$$\begin{aligned} f_{-1} &= \frac{e^2_{\varnothing\mathrm{PB}} + e^2_{\varnothing\mathrm{PQ}} + e^2_{\varnothing\mathrm{P}\varnothing}}{e^2_{\mathrm{total}}} \\ &= \frac{\dfrac{[\mathrm{P}]}{K_\mathrm{P}}}{\left(1 + \dfrac{[\mathrm{H}^+]}{K_\mathrm{H}}\right)\left(1 + \dfrac{[\mathrm{A}]}{K_\mathrm{A}} + \dfrac{[\mathrm{P}]}{K_\mathrm{P}}\right)}, \end{aligned} \tag{6}$$

$$\begin{aligned} f_3 &= \frac{e^3_{\varnothing\varnothing\mathrm{B}} + e^3_{\varnothing\mathrm{AB}} + e^3_{\varnothing\mathrm{PB}} + e^3_{\mathrm{H}\varnothing\mathrm{B}} + e^3_{\mathrm{HAB}} + e^3_{\mathrm{HPB}}}{e^3_{\mathrm{total}}} \\ &= \frac{\dfrac{[\mathrm{B}]}{K_\mathrm{B}}}{\left(1 + \dfrac{[\mathrm{B}]}{K_\mathrm{B}} + \dfrac{[\mathrm{Q}]}{K_\mathrm{Q}}\right)}, \end{aligned} \tag{7}$$

and

$$\begin{aligned} f_{-3} &= \frac{e^4_{\varnothing\varnothing\mathrm{Q}} + e^4_{\varnothing\mathrm{A}\varnothing} + e^4_{\varnothing\mathrm{PQ}} + e^4_{\mathrm{H}\varnothing\mathrm{Q}} + e^4_{\mathrm{HA}\varnothing} + e^4_{\mathrm{HPQ}}}{e^4_{\mathrm{total}}} \\ &= \frac{\dfrac{[\mathrm{Q}]}{K_\mathrm{Q}}}{\left(1 + \dfrac{[\mathrm{B}]}{K_\mathrm{B}} + \dfrac{[\mathrm{Q}]}{K_\mathrm{Q}}\right)}. \end{aligned} \tag{8}$$

The net turnover rate (reaction velocity) can be expressed as

$$v = \frac{V}{[E_{\mathrm{total}}]} = k_2\left[e^2_{\mathrm{total}}\right] - k_{-2}\left[e^3_{\mathrm{total}}\right]. \tag{9}$$

Application of the King and Altman method (see Segel (24)) to the scheme shown in Fig. 1 *B* yields the following expression for the net reaction velocity:

$$v = \frac{k_1k_2k_3k_4f_1f_3 - k_{-1}k_{-2}k_{-3}k_{-4}f_{-1}f_{-3}}{\left(\begin{array}{l} k_1k_4(k_2 + k_{-2})f_1 + k_2k_3(k_4 + k_{-4})f_3 + k_1k_3(k_2 + k_4)f_1f_3 + k_{-1}k_{-2}(k_4 + k_{-4}))f_{-1} + \\ k_{-3}k_{-4}(k_2 + k_{-2})f_{-3} + k_{-1}k_3(k_4 + k_{-4})f_{-1}f_3 + k_1k_{-3}(k_2 + k_{-2})f_1f_{-3} + k_{-1}k_{-3}(k_{-2} + k_{-4})f_{-1}f_{-3} \end{array}\right)}. \tag{10}$$

This complex expression can be obtained using the freely available KAPattern package tool for computer-aided derivation of the enzyme rate expressions (25). Substitution of the fractional occupancy distributions, defined by Eqs. 5–8, yields the following expression for the net reaction velocity in terms of the individual rate constants and dissociation constants:

$$
\begin{aligned}
v = \frac{k_1k_2k_3k_4K_PK_Q[A][B]\left[H^+\right] - k_{-1}k_{-2}k_{-3}k_{-4}K_HK_AK_B[P][Q]}{K_PK_QK_Hk_2k_3k_4[A][B] + K_PK_Qk_2k_3k_4[A][B]\left[H^+\right] + K_PK_QK_Hk_2k_3k_{-4}[A][B] + K_PK_Qk_2k_3k_{-4}[A][B]\left[H^+\right]} \\
+ K_PK_Qk_1k_3k_2[A][B]\left[H^+\right] + K_PK_Qk_1k_3k_4[A][B]\left[H^+\right] + K_PK_Qk_1k_4k_2[A][B]\left[H^+\right] + K_PK_Qk_1k_4k_{-2}[A][B]\left[H^+\right] \\
+ K_PK_Bk_2k_1k_{-3}[A]\left[H^+\right][Q] + K_PK_BK_Hk_2k_{-3}k_{-4}[A][Q] + K_PK_Bk_2k_{-3}k_{-4}[A]\left[H^+\right][Q] + K_PK_Bk_1k_4k_2[A]\left[H^+\right][Q] \\
+ K_PK_Bk_{-2}k_1k_{-3}[A]\left[H^+\right][Q] + K_PK_BK_Hk_{-2}k_{-3}k_{-4}[A][Q] + K_PK_Bk_{-2}k_{-3}k_{-4}[A]\left[H^+\right][Q] + K_PK_Bk_1k_4k_{-2}[A]\left[H^+\right][Q] \\
+ K_PK_BK_Qk_1k_4k_2[A]\left[H^+\right] + K_PK_BK_Qk_1k_4k_{-2}[A]\left[H^+\right] + K_AK_HK_Qk_4k_{-1}k_3[B][P] + K_AK_QK_Hk_4k_{-1}k_{-2}[B][P] \\
+ K_AK_HK_Qk_3k_2k_4[B][P] + K_AK_Qk_4k_2k_3[B]\left[H^+\right][P] + K_AK_QK_PK_Hk_4k_2k_3[B] + K_AK_QK_Pk_4k_2k_3\left[H^+\right][B] \\
+ K_AK_HK_Qk_{-4}k_{-1}k_3[B][P] + K_AK_QK_Hk_{-4}k_{-1}k_{-2}[B][P] + K_AK_QK_Hk_{-4}k_2k_3[B][P] + K_AK_Qk_{-4}k_2k_3[B]\left[H^+\right][P] \\
+ K_AK_QK_PK_Hk_{-4}k_2k_3[B] + K_AK_QK_Pk_{-4}k_2k_3\left[H^+\right][B] + K_AK_BK_Hk_2k_{-3}k_{-4}[P][Q] + K_AK_Bk_2k_{-3}k_{-4}\left[H^+\right][P][Q] \\
+ K_AK_BK_Hk_{-2}k_{-3}k_{-4}[P][Q] + K_AK_Bk_{-2}k_{-3}k_{-4}\left[H^+\right][P][Q] + K_AK_BK_Hk_{-1}k_{-3}k_{-2}[P][Q] + K_AK_BK_Hk_{-1}k_{-3}k_{-4}[P][Q] \\
+ K_AK_BK_Hk_{-1}k_{-2}k_4[P][Q] + K_AK_BK_Hk_{-1}k_{-2}k_{-4}[P][Q] + K_AK_BK_HK_Qk_{-1}k_{-2}k_4[P] + K_AK_BK_HK_Qk_{-1}k_{-2}k_{-4}[P] \\
+ K_AK_BK_PK_Hk_{-3}k_{-4}k_2[Q] + K_AK_BK_Pk_2k_{-3}k_{-4}\left[H^+\right][Q] + K_AK_BK_PK_Hk_{-3}k_{-4}k_{-2}[Q] + K_AK_BK_Pk_{-3}k_{-4}k_{-2}[Q]\left[H^+\right]
\end{aligned}
\tag{11}
$$

Defining kinetic constants in terms of groups of rate constants and using the Haldane relationship (24), Eq. 11 yields the following velocity equation for the mechanism of Fig. 1.

$$
\begin{aligned}
v = \frac{\left(\frac{V_1}{K_{mB}K_{ia}K_{ih}}\right)\left([A][B]\left[H^+\right] - \left(\frac{1}{K_{eq}}\right)[P][Q]\right)}{\left(\frac{K_{mH}}{K_{mB}K_{ia}K_{ih}}\right)[A][B] + \left(\frac{1}{K_{ia}K_{ih}}\right)[A]\left[H^+\right] + \left(\frac{K_{mH}}{K_{mA}K_{ih}K_{iq}}\right)[A][Q] + \left(\frac{1}{K_{mB}K_{ia}K_{ih}}\right)[A][B]\left[H^+\right]} \\
+ \left(\frac{1}{K_{ia}K_{ih}K_{iq}}\right)[A]\left[H^+\right][Q] + \left(\frac{K_{mA}}{K_{mB}K_{ia}}\right)[B] + \left(\frac{K_{mA}}{K_{mB}K_{ia}K_{ih}}\right)[B]\left[H^+\right] + \left(\frac{K_{mQ}}{K_{mP}K_{ib}K_{iq}}\right)[B][P] + \left(\frac{K_{mA}}{K_{mB}K_{ia}K_{ih}K_{ip}}\right)[B]\left[H^+\right][P] \\
+ \left(\frac{K_{mQ}}{K_{mP}K_{iq}}\right)[P] + \left(\frac{1}{K_{iq}}\right)[Q] + \left(\frac{1}{K_{mP}K_{iq}}\right)[P][Q] + \left(\frac{1}{K_{ih}K_{iq}}\right)[Q]\left[H^+\right] + \left(\frac{1}{K_{ih}K_{ip}K_{iq}}\right)\left[H^+\right][P][Q]
\end{aligned}
\tag{12}
$$

The kinetic constants in Eq. 12 are defined as

$$
V_1 = \frac{\text{num}_1}{\text{Coef}_{ABH}},\ V_2 = \frac{\text{num}_2}{\text{Coef}_{PQ}},\ K_{mA} = \frac{\text{Coef}_{BH}}{\text{Coef}_{ABH}},
$$

$$
K_{mB} = \frac{\text{Coef}_{AH}}{\text{Coef}_{ABH}},\ K_{mH} = \frac{\text{Coef}_{AB}}{\text{Coef}_{ABH}},
$$

$$
K_{mP} = \frac{\text{Coef}_{Q}}{\text{Coef}_{PQ}},\ K_{mQ} = \frac{\text{Coef}_{P}}{\text{Coef}_{PQ}},\ K_{ia} = \frac{\text{Coef}_{HQ}}{\text{Coef}_{AHQ}},
$$

$$
K_{ib} = \frac{\text{Coef}_{P}}{\text{Coef}_{BP}},\ K_{ih} = \frac{\text{Coef}_{Q}}{\text{Coef}_{HQ}},
$$

$$
K_{ip} = \frac{\text{Coef}_{BH}}{\text{Coef}_{BHP}},\ K_{iq} = \frac{\text{Coef}_{AH}}{\text{Coef}_{AHQ}},\ \text{and}\ K_{eq} = \frac{\text{num}_1}{\text{num}_2},
$$

where we have used the shorthand notation from Segel (24); for example, $\text{num}_1 = k_1k_2k_3k_4K_PK_Q$, $\text{num}_2 = k_{-1}k_{-2}k_{-3}k_{-4}K_AK_BK_H$, $\text{Coef}_{AB} = K_PK_QK_Hk_2k_3(k_4 + k_{-4})$, and so on. Other than V_1 and V_2, all of these parameters have the units of concentration (mass/unit volume); V_1 and V_2 have the units of mass/unit time/mass protein. Full definitions are presented in the Supporting Material.

For a given value of the equilibrium constant for the tri-bi biochemical reaction, the twelve kinetic parameters cannot vary independently. They are related to the equilibrium constant K_{eq} via the equilibrium relationship

$$
K_{eq} = \left(\frac{[P][Q]}{[A][B]\left[H^+\right]}\right)_{eq} = \frac{\text{num}_1}{\text{num}_2} = \frac{K_{mP}K_{iq}}{K_{mB}K_{ia}K_{ih}}\frac{V_1}{V_2}. \tag{13}
$$

In the next section, we apply the general form of the tri-bi enzyme mechanism to analyze experimental data on the kinetics of Complex I to determine whether the proposed mechanism can match the experimental data and to estimate the associated parameter values.

Kinetic model of Complex I

Complex I is the first of the respiratory complexes providing the protonmotive force required for energy-consuming processes like the synthesis of ATP in the oxidative phosphorylation process in the cell. It is an energy-converting oxidoreductase that accepts electrons from a hydride donor ($NADH^{2-}$) and passes them to a membrane-bound two-electron acceptor (ubiquinone) with translocation of four protons across the mitochondria intermembrane. The reference chemical reaction can be written as

$$
NADH^{2-} + CoQ + H_x^+ + 4H_x^+ \rightleftharpoons QH_2 + NAD^- + 4H_i^+. \tag{14}
$$

The equilibrium constant for the reference reaction ($K_{eq,C1}$) can be calculated as

$$K_{eq,C1} = \left(\frac{[NAD^-][QH_2][H_i^+]^4}{[NADH^{2-}]_{free}[CoQ][H_x^+]^5}\right)_{eq} = K_{r,eq}e^{-4F\Delta\Psi/RT} = e^{-(\Delta_rG^0_{C1}+4F\Delta\Psi)/RT}, \quad (15)$$

where $K_{r,eq}$ is the equilibrium constant and $\Delta_rG^0_{C1}$ is the standard free energy for the chemical reaction $NADH^{2-} + CoQ + H^+ \rightleftharpoons QH_2 + NAD^-$. The term $e^{-4F\Delta\Psi/RT}$ accounts for the free energy cost of pumping four protons across the inner mitochondrial membrane, where $\Delta\Psi$ is the potential difference, measured relative to the matrix, and F is Faraday's constant. The reference Gibbs free energy $\Delta_rG^0_{C1}$ is computed using the basic thermodynamic data (298.15 K, $I = 0.15$ M) listed in Xin et al. (26):

$$\Delta_rG^0_{C1} = \Delta_fG^0_{NAD^-} + \Delta_fG^0_{QH_2} - \Delta_fG^0_{NADH^{2-}} - \Delta_fG^0_{CoQ} = -0.70 + (-89.92) - 21.12 - 0.0 = -111.74\ \text{kJ/mol} \quad (16)$$

The apparent equilibrium constant is computed to include proton transfer across the membrane and $NADH^{2-}$ binding dynamics in the model, which is an explicit function of the proton gradient and electrostatic gradient across the membrane:

$$K^{app}_{eq,C1} = \frac{[NAD^-][QH_2]}{[NADH^{2-}]_{total}[CoQ][H_x^+]} = \frac{[NADH^{2-}]_{free}}{[NADH^{2-}]_{total}}\frac{[NAD^-][QH_2]}{[NADH^{2-}]_{free}[CoQ][H_x^+]} = \frac{[NADH^{2-}]_{free}}{[NADH^{2-}]_{total}}\left(\frac{[H_x^+]}{[H_i^+]}\right)^4 e^{-(\Delta_rG^0_{C1}+4F\Delta\Psi)/RT}, \quad (17)$$

where $[NADH^{2-}]_{total}$ represents the sums of free NADH ($[NADH^{2-}]_{free}$) and protein-bound NADH NADH ($[NADH^{2-}]_{bound}$).

Here, we assume simple first-order binding of NADH to protein, with the bound fraction of the binding protein $f_b = X_{bound}/X_0$ computed as $f_b = [NADH^{2-}]_{free}/(K_n + [NADH^{2-}]_{free})$. Then the amount of bound NADH is computed as $[NADH^{2-}]_{bound} = X_0f_b$, where X_0 is protein-NADH binding capacity in the matrix, and K_n is the protein-NADH binding dissociation constant. Solving for free $NADH^{2-}$ as a function of total $NADH^{2-}$, we have

$$[NADH^{2-}]_{free} = \frac{1}{2}\left([NADH^{2-}]_{total} - K_n - X_0 + \sqrt{([NADH^{2-}]_{total} - K_n - X_0)^2 + 4K_n[NADH^{2-}]_{total}}\right) \quad (18)$$

The mechanism involves both proton and electron transfers: the electron transfer from substrate $NADH^{2-}$ to ubiquinone through a number of protein-bound prosthetic groups, flavin mononucleotides (FMNs), 6-8 iron-sulfur clusters, and quinones. It has been shown that the rate of electron transfer increases with pH because the flavin potential decreases, increasing the thermodynamic driving force for electron transfer (14). To account for this effect phenomenologically, we assume that a hydrogen ion can act as a noncompetitive inhibitor of electron transfer.

Hypothesizing that the conformational change tri-bi enzyme mechanism proposed in the previous section (Fig. 1 *B*) can explain the observed kinetics (8), and the flux of Complex I can be expressed as

$$V_{c1} = \frac{\left(\frac{1}{1+\frac{[H^+]}{K_{iH}}}\right)\left(\frac{V_1}{K_{mB}K_{ia}K_{iH}}\right)\left([A][B][H^+] - \left(\frac{1}{K^{app}_{eq}}\right)[P][Q]\right)}{\left(\frac{K_{mH}}{K_{mB}K_{ia}K_{iH}}\right)[A][B] + \left(\frac{1}{K_{ia}K_{iH}}\right)[A][H^+] + \left(\frac{K_{mH}}{K_{mA}K_{iH}K_{iQ}}\right)[A][Q] + \left(\frac{1}{K_{mB}K_{ia}K_{iH}}\right)[A][B][H^+] + \left(\frac{1}{K_{ia}K_{iH}K_{iQ}}\right)[A][H^+][Q] + \left(\frac{K_{mA}}{K_{mB}K_{iA}}\right)[B] + \left(\frac{K_{mA}}{K_{mB}K_{ia}K_{iH}}\right)[B][H^+] + \left(\frac{K_{mQ}}{K_{mP}K_{ib}K_{iQ}}\right)[B][P] + \left(\frac{K_{mA}}{K_{mB}K_{ia}K_{iH}K_{ip}}\right)[B][H^+][P] + \left(\frac{K_{mQ}}{K_{mP}K_{iQ}}\right)[P] + \left(\frac{1}{K_{iQ}}\right)[Q] + \left(\frac{1}{K_{mP}K_{iQ}}\right)[P][Q] + \left(\frac{1}{K_{iH}K_{iQ}}\right)[Q][H^+] + \left(\frac{1}{K_{iH}K_{iP}K_{iQ}}\right)[H^+][P][Q]}, \quad (19)$$

where [A], [B], [P], [Q], and $[H^+]$ represent the concentrations of $NADH^{2-}$, CoQ, NAD^-, QH_2, and hydrogen ion, respectively, in the matrix. Here, CoQ and QH_2 (reactants B and Q) represent oxidized and reduced ubiquinol in a generic sense. The kinetic parameters, particularly the binding constants for these reactants, are in general expected to depend on the particular form of ubiquinol present.

Parameter estimation

The developed kinetic model has 12 adjustable parameters. Parameter values were estimated in a systematic manner in multiple steps by least-square fitting of the model-simulated outputs to the available experimental data in Figs. 2–5, as detailed in the Results section below. The FMINCON

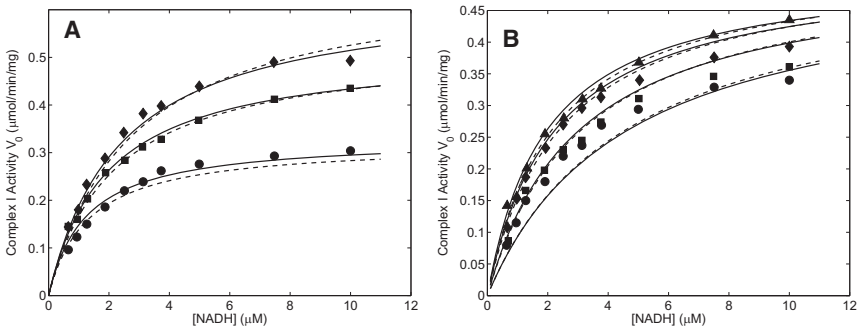

FIGURE 2 (*A*) Complex I activity as a function of $NADH^{2-}$ concentration at different Q_1 concentrations in the absence of products. Kinetic data were obtained from Fig. 4 of Nakashima et al. (8). The Q_1concentrations in the assay were 50 μM (◆), 25 μM (■), and 10 μM (●). (*B*) Complex I activity as a function of $NADH^{2-}$ concentration at different NAD^- concentrations. Kinetic data were obtained from Fig. 5 *A* of Nakashima et al. (8). The NAD^- concentrations were 0μM(▲), 20 μM (◆), 80 μM (■), and 200 μM (●) in the assay. Q_1 concentration was fixed to at 25 μM in these assays. Solid lines are results of model fitting to the data points represented by symbols based on the optimization of kinetic parameters (Table 1). Dashed lines are results of model fitting based on the optimization of rate constants and dissociation constants (Table 1).

algorithm in MATLAB (The MathWorks, Natick, MA) was used to solve this nonlinear optimization problem. In addition, sensitivity analysis was performed to estimate the sensitivity of the least-square error to small changes in parameter values. The sensitivity was computed using (27)

$$S_i = \frac{\max\left(\left|E_i^*(x_i \pm 0.1x_i) - E_i^*(x_i)\right|\right)}{0.1E_i^*(x_i)}, \qquad (20)$$

where E^* is the least-squared difference between model simulations and experimental data, and x_i is the optimized value of the ith parameter. The estimated sensitivity coefficients are listed in Table 1.

RESULTS

Kinetic parameters determination from bovine and rat mitochondrial Complex I

Nakashima et al. (8) conducted a number of experiments to study the steady-state kinetics of purified Complex I from bovine heart mitochondria, and proposed an ordered bi-bi sequential mechanism. Their data are used here to identify kinetic parameters for Complex I in bovine heart mitochondria using coenzyme Q_1 as the substrate. Figs. 2 and 3 illustrate model fits to data obtained from Figs. 4 and 5, *a–c*, of Nakashima et al. (8): Fig. 2, *A* and *B*, plots the Complex I activity versus $NADH^{2-}$ concentration at different CoQ_1 and NAD^- concentrations; Fig. 3, *A* and *B*, plots the Complex I activity as a function of CoQ_1 concentration at different NAD^- and QH_2 concentrations. All experimental data in Figs. 2 and 3 were obtained at pH 8.0 and 20°C. The reaction medium contains 0.1 M potassium phosphate and 0.1% dodecylmaltoside (8). Measured enzyme activity is expressed in μmol/min/mg protein. The ionic strength of the medium was estimated to be $I = 0.25$ M. In fitting the data in Figs. 2 and 3, the thermodynamic variables used in the model were adjusted to the experimental conditions ($T = 293.15$ K, $I = 0.25$ M) using the procedure outlined in Beard and Qian (28).

The data from Figs. 2 and 3 were used to estimate 10 of the 12 adjustable parameter values in our model for Complex I by determining values at which the model best fits the data. To do the optimization in a systematic manner in multiple steps, Fig. 4 in Nakashima et al. was used first to determine the parameters $K_{m\mathrm{A}}$, $K_{m\mathrm{B}}$, $K_{i\mathrm{h}}$, and $K_{m\mathrm{H}}$. For simplicity, we further assume that $K_{i\mathrm{h}}$ equals $K_{m\mathrm{H}}$. (Optimization was also performed without this assumption, which shows that these two parameters are not significantly different.) Using the data from Fig. 5 *c* in Nakashima

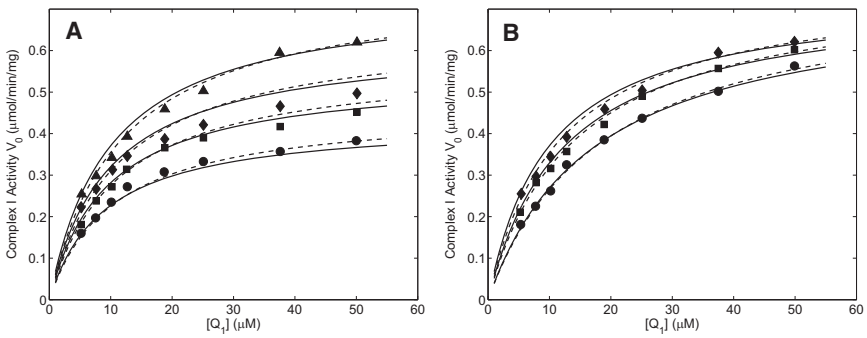

FIGURE 3 (*A*) Complex I activity as a function of Q_1 concentration at different NAD^- concentrations. Kinetic data were obtained from Fig. 5 *B* of Nakashima et al. (8). The NAD^- concentrations in the assay were 0 μM (▲), 100 μM (◆), 200 μM (■), and 400 μM (●). $NADH^{2-}$ concentration was fixed at 6 μM in these assays. (*B*) Complex I activity as a function of Q_1 at different Q_1H_2 concentrations. Kinetic data were obtained from Fig. 5 *C* of Nakashima et al. (8). Q_1H_2 concentrations in the assay were 0 μM (◆), 25 μM (■), and 75 μM (●). $NADH^{2-}$ concentration was fixed at 6 μM in these assays. Solid lines are results of model fitting to the data points represented by symbols based on the optimization of kinetic parameters (Table 1). Dashed lines are results of model fitting based on the optimization of rate constants and dissociation constants (Table 1).

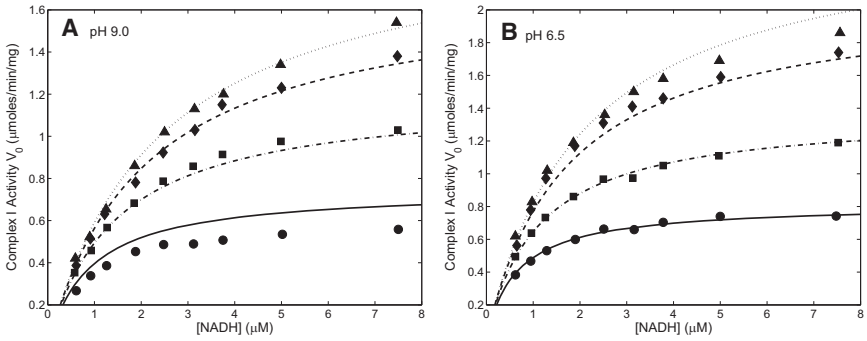

FIGURE 4 (*A*) Complex I activity as a function of NAD^- concentration at pH 9.0. Kinetic data were obtained from Fig. 1 (*upper left*) of Hano et al. (9). Symbols •, ■, ◆, and ▲ represent data obtained in the presence of 25 μM, 50 μM, 100 μM, and 150 μM DQ in the assay. No products were present in the assay. The solid, dash-dotted, dashed, and dotted lines are results of model fitting for the data points represented by symbols •, ■, ◆, and ▲, respectively. (*B*) Complex I activity as a function of NAD^- concentration at pH 6.5. Kinetic data were obtained from Fig. 1 (*upper right*) of Hano et al. (9). Symbols •, ■, ◆, and ▲ represent data obtained in the presence of 25 μM, 50 μM, 100 μM, and 150 μM DQ in the assay. No products were present in the assay. Solid, dash-dotted, dashed, and dotted lines are results of model fitting for the data points represented by symbols •, ■, ◆, and ▲, respectively.

et al., two more parameters, K_{iq} and K_{ia}, may be determined. Finally, data from Fig. 5, *a* and *b*, in Nakashima et al. were used to determine the remaining four parameters, K_{ib}, K_{ip}, K_{mP}, and K_{mQ}. Because NAD^- and QH_2 never occur together in these experiments, the [P][Q] term in the denominator of the flux expression is never nonzero. This means that our analysis is sensitive to the ratio of K_{mQ} to K_{mP}, not to the absolute values of these parameters.

The parameter values associated with the best fits of the model to the data are listed in Table 1 (*left four columns*) and the corresponding model predictions are plotted as solid lines in Figs. 2 and 3. For comparison, we also list in Table 1 the parameter values calculated by directly optimizing the rate constants $k_{\pm i}$ and dissociation constants (K_H, K_A, K_P, K_B, and K_Q). The resulting values of rate constants $k_{\pm i}$ and dissociation constants are listed in Table 1 (*right three columns*). The corresponding model fits based on direct optimization are also plotted as dashed lines in Figs. 2 and 3. Our model, based on both sets of parameter values, effectively reproduces the ordered bi-bi sequential kinetic pattern, consistent with the observation by Nakashima et al. (8).

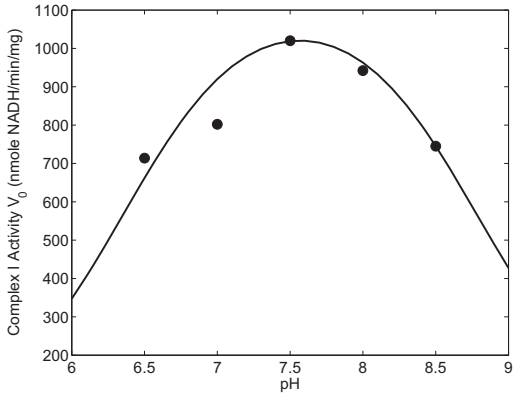

FIGURE 5 Effect of pH on the activity of Complex I from rat hearts. The measured flux as a function of pH was obtained from Fig. 2 *A* of Sadek et al. (10). The reaction medium contains 40 μM Q_1 and 40 μM $NADH^{2-}$. The solid line is the result of model fitting to the data point represented by the solid circle.

Hano et al. (9) measured the activities of Complex I from bovine heart, and studied the effect of pH on the enzyme activity using analogs of decylubiquinone (DQ) as electron acceptors. Fig. 4, *A* and *B*, shows model fits to the data obtained from Fig. 1 *A* in Hano et al. (9). The enzyme activity as a function of $NADH^{2-}$ and DQ concentrations was measured at pH 9.0 and pH 6.5 (Fig. 4, *A* and *B*, respectively). The reaction medium contained 0.2% dodecylmaltoside, and either 0.1 M pyrophosphate buffer (Fig. 4 *A*) or 0.1 M potassium phosphate buffers (Fig. 4 *B*). The ionic strength of the medium was estimated to be $I = 0.16$ M. The enzyme activity is expressed in μmol min^{-1} mg^{-1}. The parameter values associated with the best fits to the data are also listed in Table 1 (*left*) in parentheses. The estimated parameter values show that the K_m of DQ is much greater than the K_m of CoQ_1, which is consistent with the observation that DQ has a low affinity for the CoQ sites in the dehydrogenases (7). Nakashima et al. reported average kinetic parameter values for $NADH^{2-}$ and CoQ_1 of K_m = 2.07 μM and 12.72 μM, respectively. Hano et al. reported kinetic parameter values for $NADH^{2-}$ and DQ of K_m = 2.42 and 50.71 μM and 1.68 and 67.33 μM for pH 9 and pH 6.5, respectively. Those values can be directly compared to our K_m estimates of $K_{m(NADH^{2-})} = 3.10$ μM, $K_{m(CoQ_1)}$ = 17.66 μM, and $K_{m(DQ)} = 96.74$ μM.

Sadek et al. (10) conducted experiments to study the regulatory role of pH and Ca^{2+} on the activity of Complex I from rat heart mitochondria. Fig. 5 illustrates the model fits to the data obtained from Fig. 2 *A* in that study (10), which was used to estimate the value of parameter K_{ih}. Experiments were conducted at 25°C. The reaction medium contains 10 mM MOPs, 10 nM antimycin A, 20 μM KCN, and 40 μM CoQ_1. The ionic strength of the medium was estimated to be $I = 0.18$ M. The Complex I reaction was initiated by the addition of $NADH^{2-}$ (40 μM), and was measured as the rate of $NADH^{2-}$ oxidation. The measured enzyme activity is expressed in nmole $NADH^{2-}$ min^{-1} mg^{-1}. Model fits to the data are plotted as solid lines in Fig. 4. The results presented here show that the developed model is able to explain the effect of pH on enzyme activity,

TABLE 1 Estimated kinetic parameter and rate constant values for Complex I model

Kinetic parameters				Rate constants		
Name (unit)	Estimated values*	Calculated sensitivity	Calculated values†	Name (unit)‡	Estimated values	Calculated sensitivity
V_{max} (μmol min^{-1} mg^{-1})§	1.0 (3.96)	—	—	k_1 (s^{-1})	184	0.28
K_{mA} (μM)	3.10 (3.5)	3.06	—	k_2 (s^{-1})**	149	0.37
K_{ia} (μM)	0.11	0.08	0.12	k_3 (s^{-1})	148	0.92
K_{mB} (μM)	17.66 (96.74)	4.44	18.06	k_4 (s^{-1})	527	1.04
K_{ib} (μM)	13.52	0.05	20.73	k_{-1} (s^{-1})	1235	0.32
K_{mH} (pH)	8.75 (9.36)	0.94	—	k_{-2} (s^{-1})	527	1.04
K_{ih} (pH)	8.75 (9.36)	0.94	—	k_{-3} (s^{-1})	27	0.01
K_{mP} (μM)	—	—	2.29	k_{-4} (s^{-1})	149	0.37
K_{ip} (μM)	399.25	0.02	—	K_{CoQ} (μM)	27.25	4.23
K_{mQ} (μM)	43.82K_{mP}	0.11	105.08	K_{QH2} (μM)	111	0.21
K_{iq} (μM)	101.60	0.24	101.75			
K_{iih} (μM)	0.43	0.39	—			
X_0 (mM)¶	3.5	—	—			
K_n (mM)‖	0.3	—	—			

*Estimated values in parentheses are kinetic parameters for experiments using DQ as substrate.

†Parameter values were calculated from the direct optimization of rate constants$k_{\pm i}$(*right three columns*) and dissociation constants.

‡Based on definitions of the kinetic parameters $K_H = K_{ih}$ and $K_P = K_{ip}$, because we assume that $K_{mH} = K_{ih}$, we can also derive $K_A = K_{mA}$.

§We cannot estimate the value of parameter V_1 in the model without knowing the enzyme activity in the experimental setup. The value of V_{max} reported in the table is equal to$X \times V_1$, where$X$ is the enzyme activity. The optimization estimate (in μmol min$^{-1}\cdot$mg^{-1}) is $V_{max} \approx 1.0$ for Figs. 2–5 and $V_{max} \approx 4.0$ for Fig. 6.

¶The protein binding capacity for NADH^{2-}.

‖The protein-NADH binding dissociation constant.

**For simplicity, we assume that the rate constants for conformational change are the same, which means that $k_2 = k_{-4}$ and $k_{-2} = k_4$.

implying that matrix pH significantly affects the enzyme activity.

Model validation with data from bovine heart submitochondrial particles

Fato et al. (7) studied the steady-state kinetics of Complex I in bovine heart mitochondria and submitochondrial particles, and proposed a ping-pong mechanism for the enzyme. Data from Fig. 2 of their study were used here to validate the catalytic mechanisms of our model. Fig. 6 plots Complex I activity versus CoQ_1 concentration at different NADH^{2-} concentrations. All experimental data in Fig. 6 were obtained at pH 7.5 and 30°C (29). The reaction medium contains 50 mM potassium phosphate, 1 mM EDTA (29), 2 mM KCN, and 4.6 μM antimycin A (7). The ionic strength of the medium was estimated to be $I = 0.13$ M. Complex I activity was obtained spectrophotometrically by determining the change in absorbance at 240 nm (29). Measured Complex I activity is expressed in μmol min^{-1} mg^{-1} protein.

The lines plotted in Fig. 6 are model predictions using kinetic parameters from Table 1, except for V_{max}, which was allowed to vary to match the experimental data, and K_m for NADH^{2-}, which was set to 8.7 μM. This value was used (rather than 3.1 μM, estimated above) because Fato et al. conducted experiments in BHM and SMPs, not in purified enzyme conditions. Thus the apparent K_m is greater because of the NADH^{2-} binding. Our model effectively reproduced the apparent ping-pong kinetic pattern, consistent with the observations of Fato et al. (7). (Our analysis yields an estimated K_m for CoQ_1 of 17.66 μM, whereas Fato et al. reported a value of 20 μM (7).) The ability of our model to match the data without adjusting any other parameters validates the model and demonstrates its robustness.

Application to Complex I function in the intact mitochondria

To simulate Complex I operation in situ, the developed model (Fig. 1) is integrated into a biophysical model of

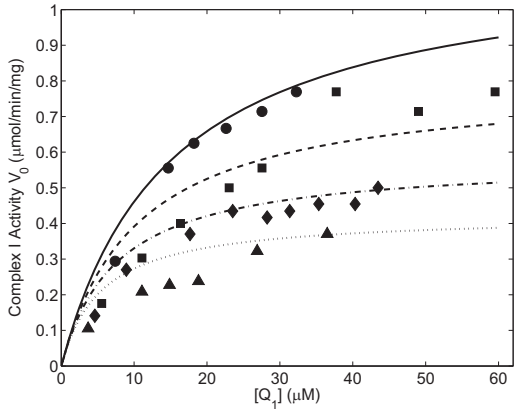

FIGURE 6 Model prediction of Complex I activity as a function of Q_1 concentration at different NADH^{2-} concentrations. Symbols ■, ◆, ▲, and • represent Complex I activity measured in the presence of 4.27 μM, 7.13 μM, 14.19 μM, and 75 μM NADH^{2-} in the assay obtained from Fig. 2 of Fato et al. (7). The solid, dashed, dash-dotted, and dotted lines are model predictions to the data points represented by the symbols •, ■, ◆, and ▲, respectively.

the mitochondrial respiratory system and oxidative phosphorylation (30). Substituting the model for Complex I into the integrated model, the new integrated model must be reparameterized to match data from the intact system. Specifically, this requires adjusting all the associated kinetic parameter values to match the same data set used for parameterization of the original model. The detailed procedure is described by Beard (30).

To incorporate charge transfer effects, it is necessary to explicitly consider the dependence of rate constants on membrane potential to account for the free energy cost of pumping four protons across the mitochondrial inner membrane. Recent electron tunneling simulations (31) and kinetics experiments (32) indicate that electrons flow rapidly from FMNs all the way down to iron-sulfur cluster N2, suggesting that the energy-converting reaction occurs at this cluster or further downstream during ubiquinone reduction. It is unlikely that the electron transfer within the $NADH^{2-}$ dehydrogenase module (I) is coupled with proton translocation, although it contains most of the known cofactors of Complex I. The role of FMNs and other cofactors in the $NADH^{2-}$ dehydrogenase module (I) may be to collect electrons and pass them to the hydrogenase module (II), so the conformational change that drives the proton translocation in the proton transporter module (III) is linked exclusively to the redox chemistry of ubiquinone reduction. That means that the proton pumping is tightly coupled with ubiquinone reduction and that binding of the substrate (product) may energetically contribute to the proton-translocation activity.

In our kinetic model (Fig. 1 *A*), the first step (*I*) represents $NADH^{2-}$ oxidation, the second step (*II*) represents electrons carried by tunneling through a chain of redox cofactors, the third step represents electrons from reduced cofactors transferring to the final acceptor, ubiquinone, to form ubiquinol, and the fourth step represents the conformational resetting of the enzyme. To account for the above assumptions, we modify the kinetic constant k_3 to $k_3 = k_3^0 \exp(-4F\Delta\Psi/RT)$, where k_3^0 is the rate constant when the membrane potential is zero. From a mechanistic perspective, this means that the last step of electron transfer to ubiquinone is accompanied by pumping protons across the membrane potential.

Fig. S1 in the Supporting Material illustrates a comparison between the new integrated model and experimentally measured values of $NADH^{2-}$, membrane potential, oxygen consumption, matrix pH, and the cytochrome c reduced fraction from Bose et al. (33). The model equations and parameter values associated with these best fits between the model simulations and experimental data are presented in the Supporting Material. The assumption $k_3 = k_3^0 \exp(-4F\Delta\Psi/RT)$ is validated by the fact that we are unable to produce reasonable matches between these data and model predictions when membrane potential dependence is incorporated into other rate constants.

DISCUSSION

A mechanistic mathematical model to explain the catalytic mechanisms of Complex I has been developed. The model assumes that the enzyme catalyzes the reaction through a four-conformation-change process. The flux expression was derived based on the general form of the tri-bi enzyme kinetic mechanism. A general form of the model provides insights into the mechanisms of Complex I activity at various pH values. The developed kinetic model was parameterized by analyzing kinetic data. In total, 10 parameters (one is the K_{mQ}/K_{mP} ratio) were estimated in a systematic manner in multiple steps by fitting the model simulation to independent data curves (see Figs. 2–5), providing quantitative estimates of the model parameters. To quantitatively measure the degree to which the curves plotted are sensitive to the parameter values, we calculated the relative sensitivities to the adjustable parameters, listed in Table 1. A high sensitivity value indicates that changing a given parameter results in significant changes to the simulated curves used to identify the parameter values. Note that three of the adjustable parameters, K_{ia}, K_{ib}, and K_{ip}, show relative sensitivity of $<10\%$, indicating that model predictions are not sensitive to these parameters around the estimated values and that these parameters may not be identified well by the analysis presented here, given the data sets analyzed. (For example, only the curves in Fig. 2 *B* and Fig. 3 *A* are sensitive to changes in K_{ib} and K_{ip}.)

Correlations in parameter estimates were investigated by computing the Hessian matrix $\partial^2 E/\partial x_i \partial x_j$. Although we cannot assign covariance estimates to our parameter estimates because we do not have information on the statistical variation in the raw data analyzed, this Hessian matrix does reveal potential correlations between our parameter estimates. Specifically, with regard to the rate constant estimates, this analysis reveals significant correlations between estimates for k_1 and k_3 and estimates for k_{-1} and k_3.

Catalytic mechanism (ordered bi-bi, random, or ping-pong?)

A number of Complex I catalytic schemes have been proposed in the literature based on steady-state kinetic experiments. Fato et al. studied the kinetics of Complex I from bovine heart membrane using CoQ_1 as the electron acceptor (7). The reciprocal plots of $1/v$ versus $1/CoQ_1$ at different $NADH^{2-}$ concentrations in that study are parallel straight lines, suggesting a random bi-bi mechanism with $NADH^{2-}$ first binding to the enzyme. Nakashima et al. also used CoQ_1 as the electron acceptor to analyze the activity of Complex I purified from bovine heart muscle (8). They proposed an ordered sequential mechanism with CoQ_1 binding as the first step and Q_1H_2 releasing as the last step.

Our analysis demonstrates a hybrid ping-pong rapid-equilibrium random bi-bi mechanism, consolidating the

characteristics from the various mechanisms and data reported in the literature. In the absence of products, our flux expression can be expressed as

$$\frac{1}{\text{flux}_{c1}}\left(\frac{V_1[H^+]}{K_{m\text{B}}K_{i\text{a}}K_{i\text{H}}}\frac{1}{1+\frac{[H^+]}{K_{i\text{H}}}}\right) = \left[\left(\frac{K_{mH}}{K_{m\text{B}}K_{i\text{a}}K_{i\text{H}}}\right)+\left(\frac{[H^+]}{K_{m\text{B}}K_{i\text{a}}K_{i\text{H}}}\right)\right]+\frac{1}{[B]}\left(\frac{[H^+]}{K_{i\text{a}}K_{i\text{H}}}\right) + \frac{1}{[A]}\left[\left(\frac{K_{m\text{A}}}{K_{m\text{B}}K_{i\text{A}}}\right)+\left(\frac{K_{m\text{A}}[H^+]}{K_{m\text{B}}K_{i\text{a}}K_{i\text{H}}}\right)\right]. \quad (21)$$

Based on this expression, at fixed pH, the model predicts the kinetic dependence of flux on substrate concentrations equivalent to that of the random bi-bi mechanism, matching the experimental observation from Fato et al. (7). The product inhibition patterns of our model are also consistent with most of the conclusions from Nakashima et al., including the competitive inhibition of QH_2 against CoQ, and the noncompetitive inhibition of NAD^- against CoQ. However, Nakashima et al. also suggested a noncompetitive inhibition of NAD^- against $NADH^{2-}$ in their model, whereas our model demonstrates that the inhibition of NAD^- against $NADH^{2-}$ is competitive. Replotting the double reciprocal lines in Fig. 5 *b* from Nakashima et al. (8), we found that the data can also be fit by lines intersecting at the $1/v$ axis. Therefore, although our model does not agree with the ordered bi-bi mechanism proposed by Nakashima et al., it is able to fit their original data fairly well.

Our model suggests that the binding of $NADH^{2-}$ and CoQ to Complex I occur in random order, and that $NADH^{2-}$ oxidation and quinine reduction are not sequentially ordered. This is supported by the experimental reports in the literature, as summarized by Hirst (34). Sled et al. reported that the redox potential of the $NADH^{2-}/NAD^-$ couple is close to the two-electron potential of the FMN (35). Zu et al. showed in protein-film voltammetry experiments that $NADH^{2-}$ and NAD^- are reversibly interconvertible at the subcomplex Iλ of mitochondrial Complex I (36). Vinogradov argued that there are two kinetically undistinguishable mechanisms for Complex I depending on the order of substrate binding and the intramolecular oxidoreduction of the enzyme itself. The relative contributions of the two pathways may depend on particular electron acceptor concentrations (37). (These two pathways correspond to the ordered bi-bi and ping-pong mechanisms.)

The model does not account for the possible presence of a diffusion-limited step in the reaction of endogenous ubiquinone with the complex. Hackenbrock et al. (38) proposed a "random collision model" for the mitochondrial respiratory chain in that the presence of diffusion control in the activity of Complex I would have important physiological implications. There are no available experimental data sets of diffusion control of Complex I interacting with exogenous ubiquinone.

pH effect

Our model predicts that the matrix pH plays an important role in the regulation of Complex I activity. Specifically, in the absence of membrane potential, Complex I activity increases and then decreases, as matrix proton concentration increases from pH 6.5 to pH 9.0 (10). The optimal pH value corresponding to the maximal activity is ~7.5. The increase in activity is due to our assumption that protons participate in $NADH^{2-}$ oxidation as substrates to transfer a hydride to Complex I. This assumption is reasonable, since the hydride transfer reaction can avoid the formation of high-energy $NADH^{2-}$ radical intermediates (34). The decrease is due to our assumption that matrix protons also act as inhibitors of the enzyme. An increase in matrix proton concentration decreases the flavin potential in Complex I, decreasing the thermodynamic driving force for electron transfer from the $NADH^{2-}$ binding end to the CoQ binding end in Complex I (14). The competition of these two effects results in the bell shape of the pH dependence relationship (Fig. 5).

Furthermore, our model indicates that matrix pH has a pronounced effect on the binding of $NADH^{2-}$ to Complex I and the maximal apparent enzyme activity. This finding differs from the conclusion from Hano et al. (9), who conducted a number of experiments to study the effect of pH on the steady-state kinetics of bovine Complex I. They assumed that the enzyme obeys the ordered sequential model proposed by Nakashima et al. (8), and obtained different values of parameters at different pH values. Based on an analysis of the changes in parameter values, Hano et al. suggested that the maximal enzyme activity at the saturating concentrations of DQ and $NADH^{2-}$ is not sensitive to pH. Yet our model includes a dependence of enzyme activity on pH, and is able to reproduce fairly well the observations from both Hano et al. (9) and Nakashima et al. (8), showing that the substrate bindings are coupled to proton uptake either for proton pumping or for the formation of the product by the mechanical conformational changes. Such conformational changes couple the pumping to the reductive or oxidative phase during the catalytic turnover. In other words, the proton pump is driven by a redox-coupled conformational change in the pumping process.

In summary, we developed a detailed kinetic model for the NADH-ubiquinone oxidoreductases (Complex I) that accounts for the electron transfer from $NADH^{2-}$ to ubiquinone through protein-bound prosthetic groups, which is coupled to the translocation of protons across the inner mitochondrial membrane as well. The kinetic mechanism in our model is modified from the ping-pong bi-bi mechanism to a tri-bi enzyme mechanism that explicitly considers the proton binding and the conformational changes

associated with charge transport inside the complex. The developed model mechanism indicates a long-range interaction between the two binding sites of the substrates, induced by tight coupling between conformational change and electron transfer involving many subunits.

SUPPORTING MATERIAL

One table, one figure, and additional references are available at http://www.biophysj.org/biophysj/supplemental/S0006-3495(10)00807-6.

The authors thank Fan Wu and Kalyan Vinnakota for advice and illuminating discussion.

This work was supported by National Institutes of Health grant HL072011.

REFERENCES

1. Brandt, U. 2006. Energy converting NADH:quinone oxidoreductase (complex I). *Annu. Rev. Biochem.* 75:69–92.
2. Lenaz, G., R. Fato, …, M. L. Genova. 2004. Mitochondrial quinone reductases: complex I. *Methods Enzymol.* 382:3–20.
3. Fearnley, I. M., J. Carroll, …, J. Hirst. 2001. GRIM-19, a cell death regulatory gene product, is a subunit of bovine mitochondrial NADH: ubiquinone oxidoreductase (complex I). *J. Biol. Chem.* 276:38345–38348.
4. Hirst, J., J. Carroll, …, J. E. Walker. 2003. The nuclear encoded subunits of complex I from bovine heart mitochondria. *Biochim. Biophys. Acta.* 1604:135–150.
5. Mamedova, A. A., P. J. Holt, …, L. A. Sazanov. 2004. Substrate-induced conformational change in bacterial complex I. *J. Biol. Chem.* 279:23830–23836.
6. Belogrudov, G., and Y. Hatefi. 1994. Catalytic sector of complex I (NADH:ubiquinone oxidoreductase): subunit stoichiometry and substrate-induced conformation changes. *Biochemistry.* 33:4571–4576.
7. Fato, R., E. Estornell, …, G. Lenaz. 1996. Steady-state kinetics of the reduction of coenzyme Q analogs by complex I (NADH:ubiquinone oxidoreductase) in bovine heart mitochondria and submitochondrial particles. *Biochemistry.* 35:2705–2716.
8. Nakashima, Y., K. Shinzawa-Itoh, …, S. Yoshikawa. 2002. Steady-state kinetics of NADH:coenzyme Q oxidoreductase isolated from bovine heart mitochondria. *J. Bioenerg. Biomembr.* 34:11–19.
9. Hano, N., Y. Nakashima, …, S. Yoshikawa. 2003. Effect of pH on the steady state kinetics of bovine heart NADH: coenzyme Q oxidoreductase. *J. Bioenerg. Biomembr.* 35:419–425.
10. Sadek, H. A., P. A. Szweda, and L. I. Szweda. 2004. Modulation of mitochondrial complex I activity by reversible Ca^{2+} and NADH mediated superoxide anion dependent inhibition. *Biochemistry.* 43:8494–8502.
11. Lambert, A. J., and M. D. Brand. 2004. Superoxide production by NADH:ubiquinone oxidoreductase (complex I) depends on the pH gradient across the mitochondrial inner membrane. *Biochem. J.* 382:511–517.
12. Ohnishi, T., and J. C. Salerno. 2005. Conformation-driven and semiquinone-gated proton-pump mechanism in the NADH-ubiquinone oxidoreductase (complex I). *FEBS Lett.* 579:4555–4561.
13. Brandt, U., S. Kerscher, …, V. Zickermann. 2003. Proton pumping by NADH:ubiquinone oxidoreductase. A redox driven conformational change mechanism? *FEBS Lett.* 545:9–17.
14. Kussmaul, L., and J. Hirst. 2006. The mechanism of superoxide production by NADH:ubiquinone oxidoreductase (complex I) from bovine heart mitochondria. *Proc. Natl. Acad. Sci. USA.* 103:7607–7612.
15. Estornell, E., R. Fato, …, G. Lenaz. 1993. Assay conditions for the mitochondrial NADH:coenzyme Q oxidoreductase. *FEBS Lett.* 332:127–131.
16. Grivennikova, V. G., and A. D. Vinogradov. 2006. Generation of superoxide by the mitochondrial Complex I. *Biochim. Biophys. Acta.* 1757:553–561.
17. Liu, Y., G. Fiskum, and D. Schubert. 2002. Generation of reactive oxygen species by the mitochondrial electron transport chain. *J. Neurochem.* 80:780–787.
18. Chance, B., and H. Baltscheffsky. 1958. Respiratory enzymes in oxidative phosphorylation. VII. Binding of intramitochondrial reduced pyridine nucleotide. *J. Biol. Chem.* 233:736–739.
19. Tischler, M. E., P. Hecht, and J. R. Williamson. 1977. Effect of ammonia on mitochondrial and cytosolic NADH and NADPH systems in isolated rat liver cells. *FEBS Lett.* 76:99–104.
20. Matsuno-Yagi, A., and T. Yagi. 2001. Introduction: complex I—an L-shaped black box. *J. Bioenerg. Biomembr.* 33:155–157.
21. Hofhaus, G., H. Weiss, and K. Leonard. 1991. Electron microscopic analysis of the peripheral and membrane parts of mitochondrial NADH dehydrogenase (complex I). *J. Mol. Biol.* 221:1027–1043.
22. Friedrich, T. 2001. Complex I: a chimaera of a redox and conformation-driven proton pump? *J. Bioenerg. Biomembr.* 33:169–177.
23. Northrop, D. B. 1969. Transcarboxylase. VI. Kinetic analysis of the reaction mechanism. *J. Biol. Chem.* 244:5808–5819.
24. Segel, I. H. 1975. Enzyme Kinetics: Behavior and Analysis of Rapid Equilibrium and Steady-State Enzyme Systems. Wiley, New York.
25. Qi, F., R. K. Dash, …, D. A. Beard. 2009. Generating rate equations for complex enzyme systems by a computer-assisted systematic method. *BMC Bioinformatics.* 10:238.
26. Li, X., R. K. Dash, …, D. A. Beard. 2010. A database of thermodynamic quantities for the reactions of glycolysis and the tricarboxylic acid cycle. *J. Phys. Chem. B.*, Epub ahead of print.
27. Wu, F., F. Yang, …, D. A. Beard. 2007. Computer modeling of mitochondrial tricarboxylic acid cycle, oxidative phosphorylation, metabolite transport, and electrophysiology. *J. Biol. Chem.* 282:24525–24537.
28. Beard, D. A., and H. Qian. 2008. Chemical Biophysics: Quantitative Analysis of Cellular System. Cambridge University Press, Cambridge, United Kingdom.
29. Yagi, T. 1990. Inhibition by capsaicin of NADH-quinone oxidoreductases is correlated with the presence of energy-coupling site 1 in various organisms. *Arch. Biochem. Biophys.* 281:305–311.
30. Beard, D. A. 2005. A biophysical model of the mitochondrial respiratory system and oxidative phosphorylation. *PLOS Comput. Biol.* 1:e36.
31. Moser, C. C., T. A. Farid, …, P. L. Dutton. 2006. Electron tunneling chains of mitochondria. *Biochim. Biophys. Acta.* 1757:1096–1109.
32. Verkhovskaya, M. L., N. Belevich, …, M. I. Verkhovsky. 2008. Real-time electron transfer in respiratory complex I. *Proc. Natl. Acad. Sci. USA.* 105:3763–3767.
33. Bose, S., S. French, …, R. S. Balaban. 2003. Metabolic network control of oxidative phosphorylation: multiple roles of inorganic phosphate. *J. Biol. Chem.* 278:39155–39165.
34. Hirst, J. 2005. Energy transduction by respiratory complex I—an evaluation of current knowledge. *Biochem. Soc. Trans.* 33:525–529.
35. Sled, V. D., N. I. Rudnitzky, …, T. Ohnishi. 1994. Thermodynamic analysis of flavin in mitochondrial NADH:ubiquinone oxidoreductase (complex I). *Biochemistry.* 33:10069–10075.
36. Zu, Y., R. J. Shannon, and J. Hirst. 2003. Reversible, electrochemical interconversion of NADH and NAD^+ by the catalytic (Iλ) subcomplex of mitochondrial NADH:ubiquinone oxidoreductase (complex I). *J. Am. Chem. Soc.* 125:6020–6021.
37. Vinogradov, A. D. 1777. 2008. NADH/NAD^+ interaction with NADH: ubiquinone oxidoreductase (complex I). *Biochim. Biophys. Acta.* (7–8):729–734.
38. Hackenbrock, C. R., B. Chazotte, and S. S. Gupte. 1986. The random collision model and a critical assessment of diffusion and collision in mitochondrial electron transport. *J. Bioenerg. Biomembr.* 18:331–368.